Bioresource Technology 247 (2018) 217–225

Contents lists available at ScienceDirect

Bioresource Technology

journal homepage: www.elsevier.com/locate/biortech

Influence of catalysts on co-combustion of sewage sludge and water hyacinth blends as determined by TG-MS analysis

Limao Huang[a], Candie Xie[a], Jingyong Liu[a,*], Xiaochun Zhang[a], KenLin Chang[a], Jiahong Kuo[a], Jian Sun[a], Wuming Xie[a], Li Zheng[a], Shuiyu Sun[a], Musa Buyukada[b], Fatih Evrendilek[b]

[a] School of Environmental Science and Engineering, Institute of Environmental Health and Pollution Control, Guangdong University of Technology, Guangzhou 510006, China
[b] Department of Environmental Engineering, Abant Izzet Baysal University, Bolu 14052, Turkey

ARTICLE INFO

Keywords:
Sewage sludge
Water hyacinth
Catalysts
Co-combustion
TG-MS

ABSTRACT

Effects of the three metal carbonates (K_2CO_3, Na_2CO_3, and $MgCO_3$) were quantified on catalytic co-combustion of the sewage sludge and water hyacinth (SW) blend using a thermogravimetric-mass spectrometric (TG-MS) analysis and kinetics modeling. The main dominating steps of the catalysts were the organic volatile matter release and combustion stage. Weighted mean values of activation energy (E_m) were estimated at 181.18 KJ·mol^{-1}, 199.76 KJ·mol^{-1}, 138.76 KJ·mol^{-1}, and 177.88 KJ·mol^{-1} for SW, SW + 5% K_2CO_3, SW + 5% Na_2CO_3, and SW + 5% $MgCO_3$, respectively. The lowest E_m occurred with SW + 5% Na_2CO_3. Overall, catalyst effect on co-combustion appeared to be negligible as indicated by Gibbs free energy (ΔG). The normalized intensities of SW + $MgCO_3$ were strongest. The addition of Na_2CO_3 and $MgCO_3$ to SW increased flue gases emissions (CO_2, NO_2, SO_2, HCN, and NH_3) of SW, whereas the addition of K_2CO_3 to SW reduced flue gases emissions from the entire combustion process.

1. Introduction

With the growth of the global economy and human population, cumulative energy demand on fossil fuels, and associated emissions of greenhouse gases have increased significantly (Gangulya et al., 2012; Edward et al., 2017; IPCC, 2014). Actual and potential impacts of global climate change on the environment stipulate the pursuit of socio-economic policies that encourage the use of alternative energy sources. Increased production of biofuels is expected to contribute to the development of sustainable energy systems in industrialized and industrializing countries (Vamvuka et al., 2009; Xu and Chen, 2013).

There is an increasing amount of feedstock devoted to obtain energy from biomass such as wood, agricultural waste, coffee ground, sewage sludge, and water hyacinth (Chen et al., 2017; Huang et al., 2016). The rapidly growing rate of global urbanization has recently increased the quantity of sewage sludge (SS) from urban waste water treatment plants (Cieslik et al., 2015). Mean annual SS output was estimated at about 30 million t (with 80% moisture content) in China in 2015 (Liu et al., 2015). Since SS is laden with toxic metals, organic pollutants, and pathogens, the emissions of flue gas from SS combustion can pose harmful effects on public and environmental health (Batistella et al., 2015). On the other hand, water hyacinth (WH) (*Eichhornia crassipes*) was reported as one of the world's top ten "invasive grasses" due to its rapid and difficult-to-control proliferation (Villamagna and Murphy, 2010). However, its rapid growth paves the way for biofuel production (Zimmels et al., 2009), bioremediation (Gangulya et al., 2012), bioethanol and gas production (Aswathy et al., 2010; Mishima et al., 2008), feed production and adsorbent preparation (Guerrero-Coronilla et al., 2015), and co-combustion or pyrolysis (Huang et al., 2016; Luo et al., 2011). Many studies have focused on the hydrogen or methane production and pyrolysis gas (Luo et al., 2011; Lin et al., 2017; Barua and Kalamdhad, 2017); however, a few studies have investigated gaseous emissions during the co-combustion with water hyacinth.

Several emission reduction methods used for SS combustion included the optimization of combustion process (Han and Bollas, 2016), and the uses of catalysts (Sutton et al., 2001), adsorbents, or the dilution of the feedstock with other less pollutant materials (Xu et al., 2017). Although emissions from catalytic co-combustion of the sewage sludge and water hyacinth blend (SW) are expected to be lower than those from fossil fuels, it needs to be quantified whether or not SS-related emissions increase human exposure to health-damaging air pollutants (Batistella et al., 2015). In so doing, kinetics behaviors of emissions during the entire co-combustion process based on the chemical composition of the biomass and the reaction conditions should be

* Corresponding author.
E-mail address: www053991@126.com (J. Liu).

http://dx.doi.org/10.1016/j.biortech.2017.09.039
Received 13 July 2017; Received in revised form 4 September 2017; Accepted 6 September 2017
Available online 09 September 2017
0960-8524/

taken into account using a combined analysis technique of thermogravimetry and mass spectrometry (TG-MS) (Zhao et al., 2011; Huang et al., 2011; Miranda et al., 2012). There are a few studies about gaseous emissions from the co-combustion to improve understanding of the kinetic behaviors and gas emission characteristics of the alternative biomass under different catalysts. Therefore, the objective of this study is to quantify the thermal, kinetic and flue gas characteristics of the catalytic co-combustion of the SW blend in response to the three metal carbonates (K_2CO_3, Na_2CO_3, and $MgCO_3$) using a TG-MS analysis and non-isothermal analyses based on the Ozawa-Flynn-Wall (OFW) kinetic iso-conversional models.

2. Methods and materials

2.1. Sampling procedures

Sewage sludge samples were collected at intervals of 0.5 and 8 h through continuous acquisition from a terminal conveyor belt in a wastewater treatment plant in Guangzhou, Guangdong Province, China. Water hyacinth samples were collected from canals surrounding Guangzhou University Mega Center, Guangzhou, Guangdong Province, China. One week after all SS and WH samples were allowed to dry naturally at room temperature in the laboratory, they were milled and sieved using a 74-μm sieve. They were then subjected to oven drying at 105 °C to reach a constant weight and stored in a desiccator for subsequent testing. The moisture contents of SS and WH were 7.57% and 9.95%, respectively. The ultimate, proximate, calorific value and ash composition analyses of SS and WH are presented in Table 1.

The three metal carbonates of K_2CO_3 (purity ≥ 99.0%), Na_2CO_3 (purity ≥ 99.8%) and $MgCO_3$ (purity: 83.68–98.32%) were chosen as the catalysts owing to their inexpensive, colorless and tasteless characteristics. These catalysts were directly purchased from commercial shops. Based on a previous study on the co-combustion of SW blend ratios (Huang et al., 2016), the SW blend ratio of 80% SS to 20% WH was chosen in this study.

2.2. Experimental set-up procedures

Thermogravimetric analyses were conducted at the three heating rates of 10, 20 and 40 °C min^{-1} at a flow rate of 50 ml min^{-1}, using a simultaneous DSC–TGA equipment (NETZSCH STA 409 PC) from 30 to 1000 °C under the air atmosphere. Approximately 8 ± 0.5 mg of the sample was used in alumina crucibles in each analysis. Prior to the start of the experiment, several preliminary experiments without the samples were conducted to obtain the baseline against which the systematic errors of the instrument itself were in turn eliminated when the experiments with the samples were started. Furthermore, the samples selected randomly in the same batch were repeated for three times in an experiment to confirm the repeatability and authenticity of the generated data, and the resultant errors were within ± 2%. The NETZSCH–T4–Kinetic 2 software was used to provide TG and derivative TG (DTG) curves. A Vario EL Cube elemental analyzer (Elementar Analysen Systeme Gmbh, Germany) and a WZR-1T-CII Microcomputer Calorimeter (Bent Instrument Co., Ltd., Chain) were used for the ultimate analysis and higher heating values of the samples.

Emissions at the heating rate of 20 °C min^{-1} were monitored using a mass spectrometer (MS) (Rigaku Thermo Mass Photo, Japan) coupled to a TGA under 20% O_2/80% He atmosphere, at a flow rate of 300 ml min^{-1}. Data were normalized so that each m/z had its own response factor (Otero et al., 2011) and the intensities of the same parent molecules (CO_2, NO_2, NO, SO_2, HCN, NH_3 and H_2O) may be compared to the different samples.

2.3. Kinetic behaviors

Kinetic data from solid-state combustion were obtained using a TGA. Solid state reactions are the complex processes involving a superposition of several elementary processes such as nucleation, adsorption, desorption interfacial reaction, and surface/bulk diffusion. The approach used in the present study to compute combustion kinetic rates was based on Arrhenius equation. The rate of transformation from solid to volatile state is generally described thus:

$$\frac{d_\alpha}{d_t} = k(T)f(\alpha) \tag{1}$$

According to Arrhenius equation:

$$k(T) = Ae^{(-E_\alpha/RT)} \tag{2}$$

where α was conversion degree; t was time; T was the reaction temperature; A was the pre-exponential factor; E_α was the apparent activation energy; and R was the universal gas constant (8.314 J/K mol^{-1}).

α was expressed as follows (Huang et al., 2016):

$$\alpha = \frac{m_0 - m_t}{m_0 - m_\infty} \tag{3}$$

where m_0 and m_∞ were the initial and final masses of the samples, respectively. m_t was the mass of the samples at time t.

Eqs. (1) and (2) were combined into the following equation:

$$\frac{d_\alpha}{d_t} = Ae^{(-E_\alpha/RT)}f(\alpha) \tag{4}$$

when heating rate (β) was introduced (°C s^{-1}):

Table 1
The ultimate, proximate, calorific value and ash composition analyses of SS and WH on an air-dried basis.

Sample	Ultimate analyses (wt%)						Proximate analyses (wt%)				$Q_{net,d}$[a] (MJ kg^{-1})
	C	H	O[b]	N	S		M[c]	V[d]	A[e]	FC[f]	
SS	24.13	3.94	12.49	4.50	0.74		7.57	40.22	46.63	5.58	10.79
WH	36.62	5.28	27.49	3.01	0.25		9.95	56.30	17.40	16.35	14.77
Ash composition analyses (wt%)											
	Na_2O	MgO	P_2O_5	Al_2O_3	SiO_2	K_2O	CaO	TiO_2	MnO	Fe_2O_3	
SS	0.14	0.25	0.23	1.59	2.81	0.04	11.20	0.20	0.05	14.28	
WH	0.18	/	0.35	0.18	0.41	14.11	0.23	0.01	0.05	0.10	

[a] $Q_{net,d}$, higher heating value on an air-dried basis.
[b] O, calculated by O = 100%–C–H–N–S–M–A.
[c] M, moisture.
[d] V, volatile matters.
[e] A, ash.
[f] FC, fixed carbon.

$$\beta = \frac{d_T}{d_t} \tag{5}$$

Eq. (4) was transformed to:

$$\beta\frac{d_\alpha}{d_T} = Ae^{(-E_\alpha/RT)}f(\alpha) \tag{6}$$

Determining thermo-kinetic behaviors of biomass allows for control over its decomposition mechanism. Kinetic parameters of reactions are necessary to accurately predict its behavior and optimize the process towards target objectives during thermal degradation (Amanda and Leandro, 2016). Non-isothermal TGA is the most common and simplest method to study the kinetic and thermodynamic properties of biomass. An iso-conversional integral method is generally used to estimate activation energy values when kinetic model of the reaction mechanism is not known. Therefore, the OFW method was applied as follows (Amanda and Leandro, 2016):

$$\ln(\beta) = C_\alpha - \frac{E_\alpha}{R\cdot T} \tag{7}$$

where C_α is the function of α; and T is the absolute temperature (K).

To determine impacts of the metal carbonate compounds on the kinetic parameters of the samples during the thermal degradation, the weighted average activation energy (E_m) was estimated and applied to analyze SW reactivity (Shao et al., 2010),

$$E_m = E_1F_1 + E_2F_2 + \ldots + E_nF_n \tag{8}$$

where E_1 to E_n are apparent activation energy at each combustion stage; and F_1 to F_n are quantities of weight losses.

OFW-based thermodynamic parameters for kinetic studies, and thermodynamic parameters for pre-exponential factor (A) in Arrhenius equation, enthalpy (ΔH), free Gibbs energy (ΔG), and changes in entropy (ΔS) were expressed using Eqs. (9) to (12) (Kim et al., 2010; Huang et al., 2016).

$$A = \beta\cdot E_\alpha e^{(E_\alpha/R\cdot T_m)}/R\cdot T_m^2 \tag{9}$$

$$\Delta H = E_\alpha - RT \tag{10}$$

$$\Delta G = E_\alpha + R\cdot T_m\cdot\ln\left(\frac{k_B\cdot T_m}{h\cdot A}\right) \tag{11}$$

$$\Delta S = \frac{\Delta H - \Delta G}{T_m} \tag{12}$$

where k_B is the Boltzmann constant (1.381×10^{-23} J/K); h is the Plank constant (6.626×10^{-34} J s); T_m is the DTG peak temperature; and β uses the heating rate of 20 °C min^{-1}.

3. Results and discussion

3.1. Thermogravimetric analysis of SW blend with or without catalysts

Mass loss (TG) and weight loss rate (DTG) curves of SW with or without 5% catalysts (K_2CO_3, Na_2CO_3, and $MgCO_3$) under the heating rate of 20 °C min^{-1} were given in Fig. 1. As can be seen in Fig. 1, the overall trends of TG–DTG curves with the catalysts were similar. Based on the four curves, the combustion process of SW can be divided into the three distinct stages. Step I (< 170 °C) was the moisture exhalation with a weight loss rate of about 4.35%. Step II (170–660 °C) corresponded to the two major stages: the release and combustion of organic volatile matter (combustion stage I) and fixed carbon (combustion stage II) including the decomposition of hemicelluloses, cellulose and lignin during which the mass of SW was rapidly lost (approximately 91.58%) (Huang et al., 2016; Luo et al., 2011). Step III (> 660 °C) was the residue decomposition. In this step, the carbonaceous residuals continued to burn at a very low rate, with a slight mass loss. The peak of the DTG curves (at 350–450 °C approximately) of SW with $MgCO_3$ mainly showed the decomposition of $(MgCO_3)_4{\cdot}Mg(OH)_2$ (at 350 °C) into MgO and CO_2. This suggests that MgO could play a catalyst role in the high temperature combustion (Yu et al., 2009).

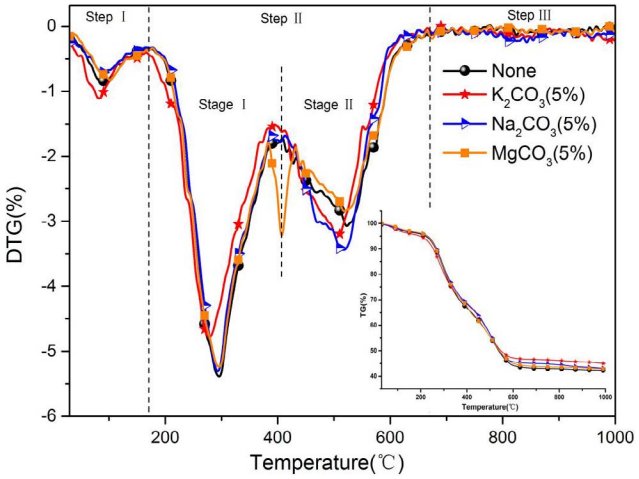

Fig. 1. TG–DTG curves of the SW blend with or without the catalysts under the heating rate 20 °C min^{-1}.

3.2. Effects of catalysts on co-combustion of SW

3.2.1. Effects of catalysts on temperature

Effects of the metal carbonates on the characteristic co-combustion temperatures of ignition temperature (T_i), and peak temperature (T_p) differed (Table 2). The non-catalyst values of T_i (T_{i1} and T_{i2}) for SW were estimated at about 242.3 °C and 463.1 °C before which the reactions with each of the catalysts already occurred. The catalyst values of T_i and T_p shifted toward the lower temperatures, and the lower the T_i value was, the better the catalytic activity was for the reaction (Shen and Qin, 2006). After the addition of the catalysts, T_i and T_p decreased to the ranges of 3.2–66.1 °C and 0.3–20.0 °C, respectively, which slightly shortened the combustion time.

As shown in Table 2, K_2CO_3 decreased both T_i and T_p up to approximately 13 °C in the low temperature stage and 20 °C in the high temperature stage, respectively. K_2CO_3 had a more positive impact on T_i and T_p of SW than did $MgCO_3$ and Na_2CO_3. All the catalysts increased the burnout temperature (T_b). Their relative strength was in the following order: Na_2CO_3 > K_2CO_3 > $MgCO_3$. This may be attributed to the different decomposition temperatures of the catalysts: K_2CO_3 (891 °C) > Na_2CO_3 (851 °C) > $MgCO_3$ (350 °C). The mineral contents of the catalysts can lead to ash deposition on the heating surface during the biomass co-combustion (Muhammad et al., 2012), thus increasing burnout temperature (T_b). Those mineral contents may cause the corrosion of the incinerator surface (Muhammad et al., 2012).

As far as the catalytic mechanism of the alkali metal carbonates is concerned, many studies found that the carbonates catalysts affected oxygen transfer in the combustion process (Shen and Qin, 2006; Yu

Table 2
Characteristic co-combustion temperatures for SW under the heating rate of 20 °C min^{-1}

Samples	T_i[a] (°C)		T_p[b] (°C)		T_b[c] (°C)
	T_{i1}	T_{i2}	T_{p1}	T_{p2}	
SW	242.3	463.1	296.2	524.0	645.59
SW + K_2CO_3	229.0	443.2	283.0	504.0	860.20
SW + Na_2CO_3	239.1	452.2	293.0	517.0	829.30
SW + $MgCO_3$	237.9	397.0	295.9	514.0	657.80

[a] T_i: onset temperature for volatile release;
[b] T_p: temperature associated with R_p;
[c] T_b: temperature of 98% conversion.

et al., 2009; Fan et al., 2016). The sludge catalytic combustion is the process of heterogeneous catalysis reaction. The catalyst activity is attributed to the electrons (or holes) and electron transfer trend. The surface activity center is considered to be the unsaturated ion ligand (oxide). If potassium carbonate is taken as an example, potassium may bond with oxygen-containing functional groups, thus leading to the migration of electron on SW surface due to its electron-donating effect. This in turn causes such phenomena as changed electron cloud distribution of carbon atoms on the SW surface, weakened intermolecular interaction of C—C or C—H bond, enhanced bonding force of C—O, and better reactivity of SW surface by an oxygen transfer mechanism, so as to facilitate the combustion process (Fang et al., 2017; Jiang et al., 2016). The theoretical reaction is as follows (Huhn et al., 1983):

$$M_2CO_3 + 4\ C \rightarrow 2\text{'MC'} + 3CO \quad (13)$$

$$\text{'MC'} + CO_2 \rightarrow \text{'MCO'} + CO \quad (14)$$

$$\text{'MCO'} + C \rightarrow \text{'MC'} + CO \quad (15)$$

where M is the alkali metal; 'MC' is the reduced state, and 'MCO' is the oxidized state.

The alkali metal carbonates boost the catalytic role of the sample surface by changing the energy distribution. Thus, their catalysis is an oxidation-reduction process. The catalytic reaction effect improves the reaction rate of coke-CO_2, thus reducing the dependence of the reaction temperature on coke (Jiang et al., 2016; Kopyscinski et al., 2014). This in turn makes the reaction temperature shift toward the lower temperatures, thus achieving the goal of the mild combustion.

3.2.2. Effects of catalysts on SW mass conversion

To illustrate the effects of the metal carbonates on SW mass conversion, the deviation was calculated using the following equation (Haykiri-Acma and Yaman, 2010):

$$\text{Deviation}(\%) = \left[\frac{TG_{exp} - TG_{cal}}{TG_{cal}}\right] \times 100 \quad (16)$$

where TG_{exp} is the mass loss of the SW samples with the addition of the metal carbonates, while TG_{cal} is calculated using the average weight of SW and catalyst at the same temperature (Huang et al., 2016; Deng et al., 2016). The greater the deviation curves were, the stronger the effect of the addition of the catalysts was on the co-combustion process (Fig. 2) (Haykiri-Acma and Yaman, 2010). The catalytic effect of Na_2CO_3 on the mass loss of SW was the most obvious ($MgCO_3$ < K_2CO_3 < Na_2CO_3). The addition of K_2CO_3 and Na_2CO_3 clearly enhanced the SW conversion at both combustion stages I (approximately 170–400 °C) and II (approximately 450–660 °C) with about 5–20% deviation of K_2CO_3 and 10–45% deviation of Na_2CO_3, respectively. For the SW + $MgCO_3$ sample, $MgCO_3$ enhanced the SW conversion at the low temperatures between 180 and 500 °C and inhibited the SW decomposition at high temperatures above 500 °C. The catalysts mainly affected the SW mass conversion at the combustion stage I, while the main dominating steps of the carbonate catalysts included the release of organic volatile matter, and combustion stage. Similar findings were also reported in related literature about alkali lignin pyrolysis and gasification with NaOH and Na_2CO_3 (Guo et al., 2012).

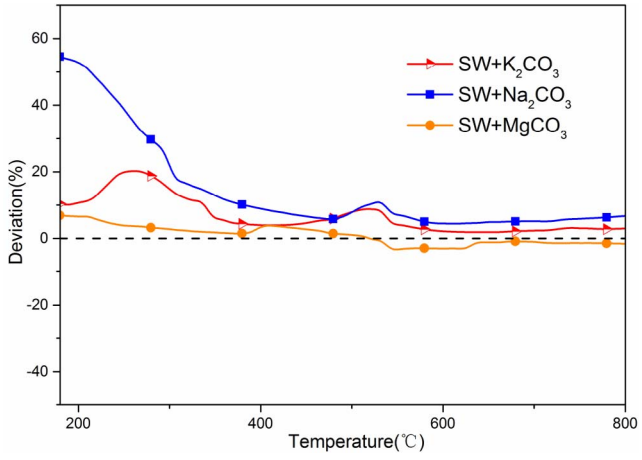

Fig. 2. Deviation curves of the effectiveness of the three metal carbonates as the catalysts for the SW conversion.

3.2.3. Effects of catalyst mass percentage on SW co-combustion

To explore effects of the catalyst mass percentage on the co-combustion characteristics of SW, the co-combustion process with the addition of K_2CO_3 was further analyzed. With the increased catalyst mass percentage, a lower temperature (T_{p1}) was needed to reach the peak of the DTG curves; in other words, ignition became easier. Thus, the curves gradually shifted to a lower temperature range (Fig. 3). With the increased K_2CO_3 mass percentage from 0% to 7%, T_{i1} decreased from 242.3 to 226.0 °C, while T_{p1} decreased from 296.2 to 273.0 °C (Table 3). This case revealed that the combustion temperature can be decreased by applying a higher catalyst ratio, thus saving energy. The peak that corresponded to biochar combustion (R_{p2}) became more apparent, and the corresponding temperature (T_{p2}) decreased. Similar findings were also reported in a previous study for biomass co-combustion (Yu et al., 2008; Sebestyén et al., 2017).

The α values of SW with the catalysts in the lower temperature range were higher than those of SW without the catalysts no matter what the catalyst quantities were. The α values at 300 °C increased in the following order: 0% K_2CO_3 < 1% K_2CO_3 < 3% K_2CO_3 < 5% K_2CO_3 < 7% K_2CO_3. While the residual mass (M_r, %) of SW with the catalysts at 1000 °C was higher than that of SW without the catalysts. This appears to be attributable to the K_2CO_3 content which can result in ash deposition on the heating surface during the biomass co-combustion (Muhammad et al., 2012) and to the remaining thermal decomposition product of K_2CO_3 such as C-K_2O (Jiang et al., 2016).

3.2.4. Effects of catalysts on co-combustion characteristic index of SW

To evaluate effects of the catalysts on SW, such characteristic co-combustion parameters as T_i,T_p,T_b, maximum weight loss rate (R_p), and average weight loss rate (R_v) are required and can be determined directly from the TG–DTG curves. In addition, *CCI* is recommended as one of the combustion performance parameters to evaluate the combustion performance of SW with the catalysts and can be calculated as a function of the characteristic temperatures and reaction rates thus (Zhuo et al., 2017):

$$CCI = \frac{(-R_p) \times (-R_v)}{T_i^2 \times T_b} \quad (17)$$

For combustion with a series of stages, *CCI* in Eq. (17) could be rewritten into Eq. (18):

$$CCI = \sum_{i=1}^{n} \delta_i CCI_i \quad (18)$$

where δ_i is the mass loss percentage of each stage in the total mass loss (%); CCI_i is *CCI* of each stage; and *CCI* is *CCI* of all stages.

The addition of $MgCO_3$ to SW increased *CCI* to $3.54\%^2\,K^{-3}\cdot min^{-2}$, when compared to $3.36\%^2\,K^{-3}\cdot min^{-2}$ without the catalysts, whereas 5% Na_2CO_3 and 5% K_2CO_3 did not improve *CCI* (Table 4). *CCI* was estimated at $3.08\%^2\,K^{-3}\,min^{-2}$ for SW + 5% K_2CO_3 and $3.33\%^2\,K^{-3}\cdot min^{-2}$ for SW + 5% Na_2CO_3 which were about $0.28\%^2\,K^{-3}\cdot min^{-2}$ and $0.03\%^2\,K^{-3}\cdot min^{-2}$ less than SW, respectively. The effects of the catalysts were in the following increasing order: K_2CO_3 < Na_2CO_3 < $MgCO_3$, while the effects of K_2CO_3 quantity on *CCI* were in the following increasing order: 5% K_2CO_3 < 0% K_2CO_3 < 7% K_2CO_3 < 3% K_2CO_3 < 1% K_2CO_3. This revealed that

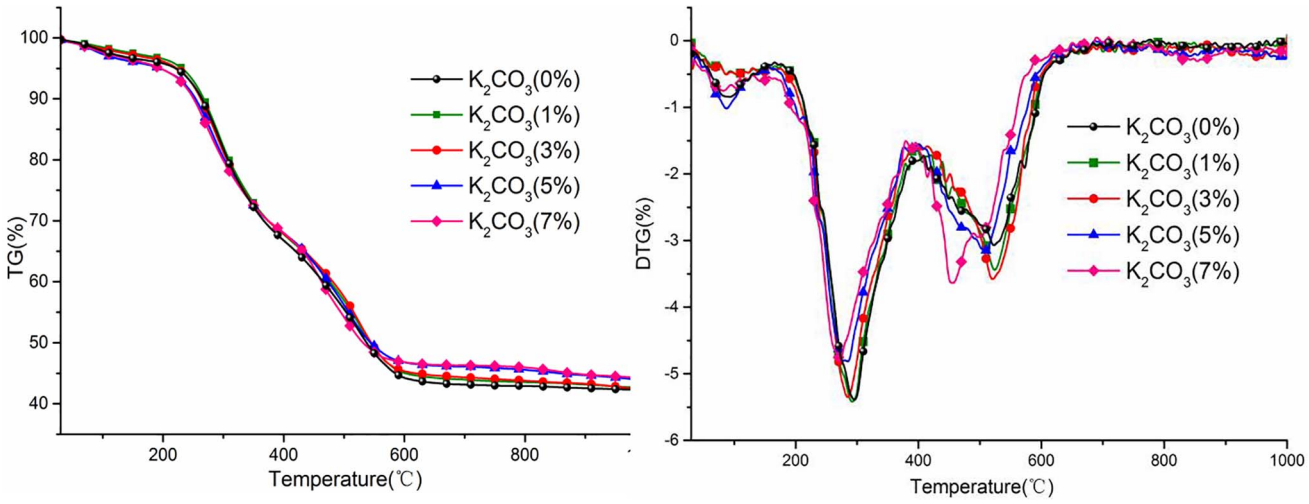

Fig. 3. TG–DTG curves of SW with K_2CO_3 in different mass percentages under the heating rate of 20 °C min^{-1}.

Table 3
Effects of K_2CO_3 mass percentages on co-combustion characteristics of SW.

Catalyst mass percentage	T_{i1} (°C)	T_p (°C)		R_p[a] (%·min^{-1})		R_v[b] (%·min^{-1})	M_r[c] (%)	α At 300 °C	T_b (°C)
		T_{p1}	T_{p2}	R_{p1}	R_{p2}				
SW	242.3	296.2	524.0	5.39	3.07	1.229	42.30	0.3137	645.59
SW + 1% K_2CO_3	239.7	291.1	523.0	5.41	3.44	1.218	42.66	0.3161	725.60
SW + 3% K_2CO_3	236.0	284.2	520.0	5.35	3.58	1.221	42.37	0.3241	845.91
SW + 5% K_2CO_3	229.0	283.0	504.0	4.81	3.16	1.194	43.77	0.3481	860.20
SW + 7% K_2CO_3	226.0	273.0	456.0	4.78	3.64	1.188	44.16	0.3598	863.02

[a] R_p: the maximum weight loss rate.
[b] R_v: average mass loss rate.
[c] *Mr*: residual mass at 1000 °C.

with the increased quantity of the catalysts, the samples did not burn more vigorously, and the biochar did not burn faster. Similar findings were also reported by the studies on the catalytic combustion of rice and wheat straw (Yu et al., 2009).

3.3. Kinetic and thermodynamic analyses

The kinetics behaviors of SW with and without the catalysts in this study were estimated using the iso-conversional method under the heating rates of 10, 20 and 40 °C min^{-1}. As can be seen in Fig. 4, E_a had high coefficients of determination (r^2) values ranging from 0.896 to 1.0 when $0.20 < \alpha < 0.90$ which in turn showed that the E_a estimates were reliable. According to Eqs. (7–12), E_a,A, ΔH, ΔG, ΔS, and E_m of SW were estimated as shown in Table 5.

The co-combustion process of SW with or without the metal carbonates occurred at the two major combustion stages with various relative mass loss quantities (Table 5). In the low temperature region, the relative mass loss quantity of SW varied between 48.17% and 51.76% with the addition of the metal carbonates. In the high temperature region, the relative mass loss content of SW ranged from 39.96% to 45.13%. E_m values were estimated at 181.18 kJ·mol^{-1}, 199.76 kJ·mol^{-1}, 138.76 kJ·mol^{-1}, 177.88 kJ·mol^{-1} for SW, SW + 5% K_2CO_3, SW + 5% Na_2CO_3, and SW + 5% $MgCO_3$, respectively. Na_2CO_3 and $MgCO_3$ decreased E_m of SW, and Na_2CO_3 had a more significant catalytic effect on the co-combustion process than did K_2CO_3 and $MgCO_3$, as was reported in Section 3.2.2.

The addition of the metal carbonates catalysts to SW can weaken C–C bond, thus reducing the entire reaction activation energy and temperature of the co-combustion reactions (Shen and Qin, 2006). Variations in E_a and A indicated that the addition of the metal carbonates appeared to change the chemical structure of SW, with metal carbonate-dependent catalytic characteristics in the different

Table 4
Co-combustion characteristics for SW with the catalysts under the heating rate of 20 °C min^{-1}.

Samples	Combustion stage I					Combustion stageII					
	T_{i1} (°C)	R_{p1} (%/min)	R_{v1} (%/min)	T_{b1} (°C)	CCI_1 (1 0 $^{-7}$)	T_{i2} (°C)	R_{p2} (%/min)	R_{v2} (%/min)	T_{b2} (°C)	CCI_2(1 0 $^{-7}$)	CCI[a] (1 0 $^{-7}$)
SW	242.3	5.39	2.701	404.0	6.13	463.1	3.07	2.075	645.6	0.46	3.36
SW + 5% K_2CO_3	229.0	4.81	2.522	390.5	5.92	443.2	3.16	1.721	650.0	0.43	3.08
SW + 5% Na_2CO_3	239.1	5.31	2.610	387.0	6.26	452.2	3.44	1.995	632.1	0.53	3.33
SW + 5% $MgCO_3$	237.9	5.23	2.840	383.0	6.85	397.0	3.22	1.784	666.3	0.55	3.54
SW + 1% K_2CO_3	239.7	5.41	2.853	395.0	6.80	446.5	3.44	1.864	652.4	0.49	3.78
SW + 3% K_2CO_3	236.0	5.35	2.694	403.1	6.42	438.1	3.58	1.817	656.1	0.52	3.63
SW + 7% K_2CO_3	226.0	4.78	2.590	384.2	6.31	419.0	3.64	1.713	651.3	0.55	3.47

[a] *CCI* is comprehensive combustion index expressed in $\%^2 \cdot K^{-3}$ min^{-2}.

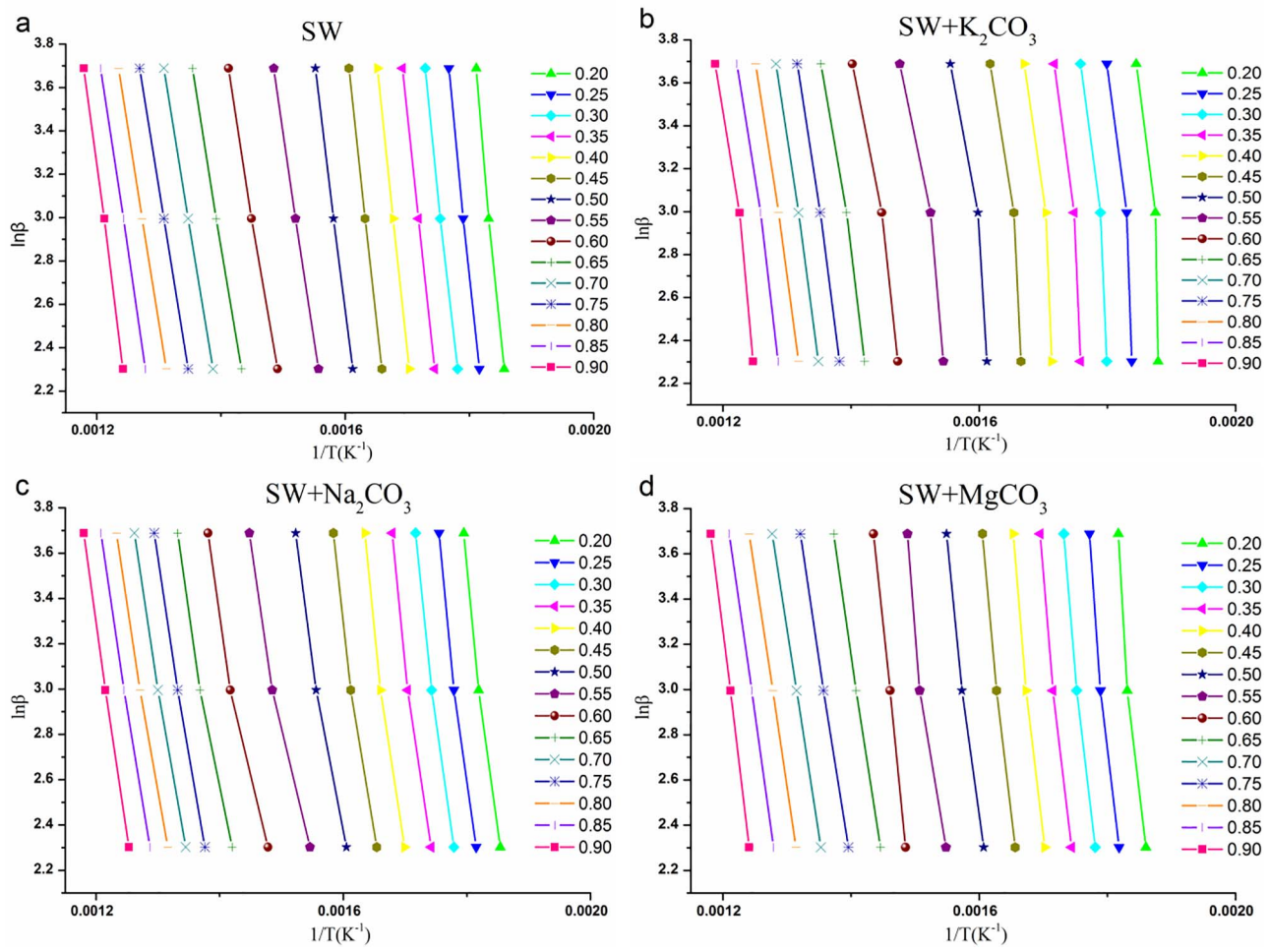

Fig. 4. Plots to determine activation energy (E_a) values for: (a) SW, (b) SW + K_2CO_3, (c) SW + Na_2CO_3, and (d) SW + $MgCO_3$ under different values of the catalytic mass conversion (α)

Table 5
Kinetic parameters of SW co-combustion with or without 5% metal carbonates under the heating rate of 20 °C min^{-1}.

Samples	Temperature range (K)	T_m (K)	A (s^{-1})	E_a (KJ/mol)	H (KJ/mol)	S (J/mol)	G (KJ/mol)	F (wt%, daf)	E_m (KJ/mol)
SW	175–403	569.35	1.77×10^{18}	216.04	211.31	90.73	159.65	51.76%	181.18
	403–683	797.15	1.19×10^{8}	153.96	147.33	−106.79	232.46	45.13%	
SW + 5%K_2CO_3	164–394	556.15	2.68×10^{20}	233.67	229.05	132.67	155.26	49.06%	199.76
	394–637	777.15	5.29×10^{9}	173.50	167.04	−75.05	225.37	39.96%	
SW + 5%Na_2CO_3	175–401	566.15	6.17×10^{13}	167.65	169.94	5.43	159.87	49.24%	138.76
	401–627	790.15	1.19×10^{7}	138.10	131.53	−125.84	230.96	40.70%	
SW + 5%$MgCO_3$	175–384	569.05	1.46×10^{19}	225.70	220.97	108.28	159.35	48.17%	177.88
	384–661	787.15	3.34×10^{9}	172.91	166.37	−78.98	228.54	40.00%	

Table 6
The normalized intensities of the samples under the heating rate of 20 °C min^{-1}.

Samples	Normalized intensities (10^{-6} A/g)						
	CO_2	H_2O	NH_3	NO	HCN	NO_2	SO_2
SW	36,850	21,990	6874	1560	1407	159	140
SW + K_2CO_3	283.83	120.13	66.34	14.09	2.07	1.17	0.96
SW + Na_2CO_3	170,000	12,380	30,420	7412	1834	714	170
SW + $MgCO_3$	188,124	14,834	37,189	9357	7011	809	630

temperature ranges. In the range of homologous temperature, the addition of Na_2CO_3 led to the lowest E_a and E_m and also decreased A relative to the control (without the catalysts) conditions. Therefore, in terms of the kinetic parameters, SW + Na_2CO_3 appeared to be the best catalyst choice for the SW co-combustion.

As shown in Table 5, the change in the enthalpies agreed with the activation energies. The changes in ΔH at the different combustion stages are due to the energy difference between the reagent and the complex activated species (Xu and Chen, 2013). The positiveΔH values showed that an external source of energy was required to raise the energy level of the reagents to their transition state (Table 5). This in turn suggested that higher enthalpy values indicated a less reactive system. According to Table 5, lower heat energies were required for Na_2CO_3 than for the K_2CO_3 and $MgCO_3$ to oxidize the reagents. ΔH values of SW in the two temperature ranges were estimated at 211.31 kJ·mol^{-1} and 147.33 kJ·mol^{-1} without the catalysts, 169.94 kJ·mol^{-1} and 131.53 kJ·mol^{-1} with Na_2CO_3, 229.05 kJ·mol^{-1} and 167.04 kJ·mol^{-1} with K_2CO_3, and 220.97 kJ·mol^{-1} and 166.37 kJ·mol^{-1} with $MgCO_3$, respectively. Thus, the formation of activated complexes was more favored with Na_2CO_3.

Entropy (ΔS) as a measure of disorder is associated with the

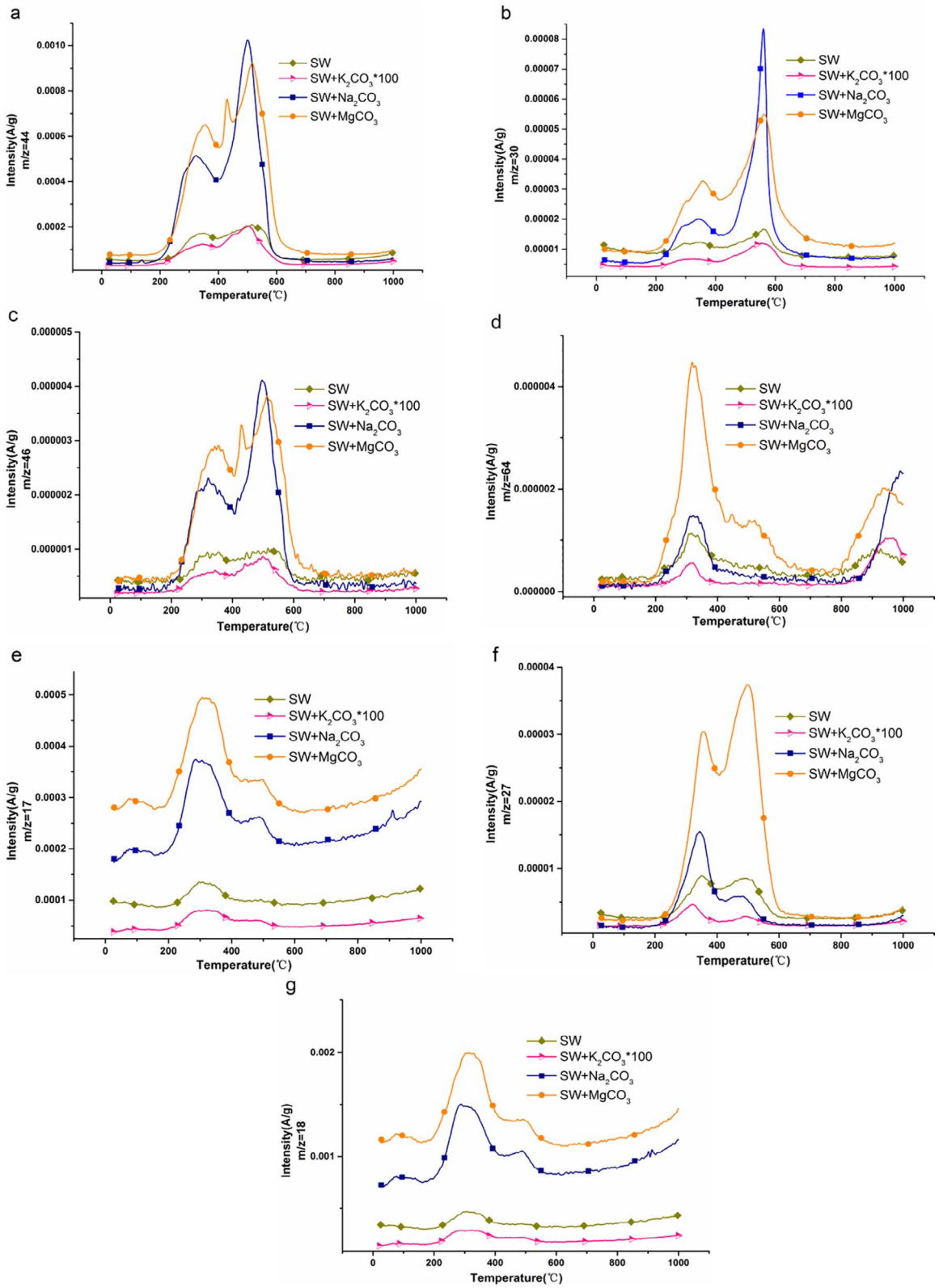

Fig. 5. Gaseous emission curves obtained by MS at the heating of 20 °C min^{-1} of SS, WH, SW and SW + K_2CO_3.

formation of complex activated species. As shown in Table 5, ΔS was positive in the low temperature range and negative in the high temperature range. Negative values indicated that the disorder degree of products formed through bond dissociations was lower than that of the initial reactants (Amanda and Leandro, 2016).

The change in Gibbs free energy (ΔG) pointed to the total energy increase in the system under the reagents, and the formation of the activated complex (Amanda and Leandro, 2016). As a comprehensive evaluation of the heat flow and disorder change, a higher ΔG value indicated a lower favorability of reaction. The catalysts could improve the ΔG value slightly which suggested that the effects of the catalysts on the overall co-combustion were negligible.

3.4. Evolved gas analysis

To determine the release of gaseous species as a result of the SW co-combustion with the catalysts, the evolved gases were simultaneously monitored using a quadruple MS during the TGA test. It can be concluded that gaseous products were mainly composed of light volatiles such as NH_3 and H_2O ((m/z) = 17 and 18), hydrocarbons such as CH_4, C_2H_2 and C_2H_4 ((m/z) = 16, 26 and 28), carbon oxides such as CO and CO_2 ((m/z) = 28 and 44), alcohols such as C_2H_5OH ((m/z) = 46), nitrogen compounds such as NO and NO_2 ((m/z) =30 and 46), aromatic compounds such as C_5H_4 ((m/z) = 64), and sulphur compounds such as COS and SO_2 ((m/z) = 60 and 64). Particular care must be taken when reporting some ions as they could belong to various compounds. For example, ions with m/z = 30 were related to the evolution of such compounds as NO, primary amines (CH_4N) and C_2H_6. Ions with m/z = 27 could be assigned to HCN or C_2H_3 ions, and m/z = 17 represented OH^- fragment of H_2O in addition to NH_3.

Table 6 shows the normalized intensities of CO_2, NO_2, SO_2, HCN, NH_3 and H_2O emissions during the co-combustion which are equal to integrated areas for the total ion current with respect to temperature (in Fig. 5) by sample mass. As shown in Table 6, the intensities of SO_2 and NO_x emissions were much lower than that of CO_2 emission during the co-combustion which was in close agreement with the proximate and ultimate analyses (Table 1). The co-combustion released H_2O, CO_2 and NH_3 majorly. The normalized intensities increased in the following order: SW + K_2CO_3 < SW + Na_2CO_3 < SW + $MgCO_3$ which corresponded to *CCI* estimated in Section 3.2.4. Small amounts of CO and CH_4 were also observed but were not shown here due to the coincidence of N_2 and O ions. The ion intensity profiles of the different emissions detected followed the trend described in the DTG curves (Fig. 1) and were generated in the two stages (Fig. 5) during volatiles and char combustion, although the width of the characteristic peaks was different for each particular compound. Similar findings were also reported in previous studies about gas emissions from co-combustion of grape pomace (Miranda et al., 2012). Continuous releases of CO_2, NO_x and SO_2 occurred during the entire combustion process, with CO_2 and NO_x being released primarily in the higher temperature range (approximately 450–700 °C) (Fig. 5a–c). NH_3 and SO_2 were mostly released in the lower temperature range (approximately 200–400 °C) (Fig. 5d and e). NH_3 emissions from the SW co-combustion began to be evolved at 180 °C and reached its maxima at 200–420 °C. SO_2 emissions began at 200 °C and reached its maxima at 200–450 °C.

As shown in Fig. 5, adding K_2CO_3 to SW obviously reduced the gas emissions, and the emissions peaked towards the low temperature. This case revealed that the K_2CO_3 catalyst was very effective in reducing the flue gases during the co-combustion process. Similar findings were also reported in related literature about the catalysts gasification of biomass (Sutton et al., 2001). With the addition of the Na_2CO_3 and $MgCO_3$ catalysts, gaseous emissions increased and peaked slightly towards the lower temperature which suggested that the Na_2CO_3 and $MgCO_3$ catalysts can promote the SW co-combustion. CO_2 emissions (Fig. 5a) at approximately 400 °C were due to the decomposition of $(MgCO_3)_4{\cdot}Mg(OH)_2$ which corresponded to the mass loss curve of SW + $MgCO_3$ in Fig. 1. NO_2 emissions at approximately 400 °C in Fig. 5c were most likely to result from the decomposition of $(MgCO_3)_4{\cdot}Mg(OH)_2$ promoting nitrides of the sludge reactions to NO_2.

4. Conclusion

The main dominating steps of the carbonate catalysts on SW were the organic volatile matter release and combustion stage. Based on the E_m values of SW (181.18 kJ·mol^{-1}), SW + K_2CO_3 (199.76 kJ·mol^{-1}), SW + Na_2CO_3 (138.76 kJ·mol^{-1}), and SW + $MgCO_3$ (177.88 kJ·mol^{-1}), Na_2CO_3 appeared to be the best catalyst for the SW co-combustion. Effects of the carbonate catalysts on the overall co-combustion were found negligible. Adding Na_2CO_3 and $MgCO_3$ to SW increased emissions from SW, respectively. However, adding K_2CO_3 catalyst to SW reduced the formation of pollutants (CO_2, NO_2, SO_2, HCN and NH_3) from the whole combustion process.

Acknowledgements

This work was financially supported by the Scientific and Technological Planning Project of Guangzhou, China (No.201704030109; 2016201604030058), the Science and Technology Planning Project of Guangdong Province, China (2017A050501036; No. 2015B020235013; 2014A050503063; 2017A040403045), and the Guangdong Special Support Program for Training High Level Talents (No. 2014TQ01Z248).

References

Amanda, A.D.M., Leandro, C.M., 2016. Kinetic parameters of red pepper waste as biomass to solid biofuel. Bioresour. Technol. 204, 157–163.
Aswathy, U.S., Sukumaran, R.K., Devi, G.L., Rajasree, K.P., Singhania, R.R., Pandey, A., 2010. Bio-ethanol from water hyacinth biomass: an evaluation of enzymatic saccharification strategy. Bioresour. Technol. 101, 925–930.
Barua, V.B., Kalamdhad, A.S., 2017. Effect of various types of thermal pretreatment techniques on the hydrolysis, compositional analysis and characterization of water hyacinth. Bioresour. Technol. 227, 147–154.
Batistella, L., Silva, V., Suzin, R.C., Virmond, E., Althoff, C.A., Moreira, R.F.P.M., José, H.J., 2015. Gaseous emissions from sewage sludge combustion in a moving bed combustor. Waste Manage. 64, 430–439.
Chen, J.C., Liu, J.Y., He, Y., Huang, L.M., Sun, S.Y., Sun, J., Chang, K.L., Kuo, J.H., Huang, S.S., Ning, X.A., 2017. Investigation of co-combustion characteristics of sewage sludge and coffee grounds mixtures using thermogravimetric analysis coupled to artificial neural networks modeling. Bioresour. Technol. 225, 234–245.
Cieslik, B.M., Snik, J.N., Konieczka, P., 2015. Review of sewage sludge management: standards, regulations and analytical methods. J. Clean. Prod. 90, 1–15.
Climate Change, 2014. Synthesis Report, Contribution of Working Groups I, II and III to the Fifth Assessment Report of the Intergovernmental Panel on Climate Change, 2014, IPCC, Geneva, Switzerland.
Deng, S.H., Wang, X.B., Tan, H.Z., Mikulcicb, H., Yang, F.X., 2016. Thermogravimetric study on the co-combustion characteristics of oily sludge with plant biomass. Thermochim Acta 633, 69–76.
Edward, F., Marcello, C., Jorge, B., Baltasar, M., Mark, W., Nilay, S., 2017. The unstudied barriers to widespread renewable energy deployment: fossil fuel price responses. Energ. Policy 103, 258–264.
Fan, S.M., Xu, L.H., Kang, T.J., Kim, H.K., 2016. Application of eggshell as catalyst for low rank coal gasification: experimental and kinetic studies. J. Energy Inst. Online http://www.journals.elsevier.com/journal-of-the-energy-institute.
Fang, S.W., Yu, Z.S., Lin, Y., Lin, Y.S., Fan, Y.L., Liao, Y.F., Ma, X.Q., 2017. A study on experimental characteristic of co-pyrolysis of municipal solid waste and paper mill sludge with additives. Appl. Therm. Eng. 111, 292–300.
Gangulya, A., Chatterjee, P.K., Dey, A., 2012. Studies on ethanol production from water hyacinth-a review. Renew. Sust. Energ. Rev. 16, 966–972.
Guerrero-Coronilla, I., Morales-Barrera, L., Cristiani-Urbina, E., 2015. Kinetic, isotherm and thermodynamic studies of amaranth dye biosorption from aqueous solution onto water hyacinth leaves. J. Environ. Managa. 152, 99–108.
Guo, D.L., Wu, S.B., Liu, B., Yin, X.L., Yang, Q., 2012. Catalytic effects of NaOH and Na_2CO_3 additives on alkali lignin pyrolysis and gasification. Appl. Energ. 95, 22–33.
Han, L., Bollas, G.M., 2016. Dynamic optimization of fixed bed chemical-looping combustion processes. Energy 112, 1107–1119.
Haykiri-Acma, H., Yaman, S., 2010. Interaction between biomass and different rank coals during co-pyrolysis. Renew. Energ. 35, 288–292.
Huang, Y.F., Kuan, W.H., Chiueh, P.T., Lo, S.L., 2011. Pyrolysis of biomass by thermal analysis-mass spectrometry (TA-MS). Bioresour. Technol. 102, 3527–3534.
Huang, L.M., Liu, J.Y., He, Y., Sun, S.Y., Chen, J.C., Sun, J., Chang, K.L., Kuo, J.H., Ning, X.A., 2016. Thermodynamics and kinetics parameters of co-combustion between sewage sludge and water hyacinth in CO2/O2 atmosphere as biomass to solid biofuel. Bioresour. Technol. 218, 631–642.
Huhn, F., Klein, J., Jüntgen, H., 1983. Investigations on the alkali–catalysed steam gasification of coal: kinetics and interactions of alkali catalyst with carbon. Fuel 62, 196–199.
Jiang, L., Hu, S., Xu, K., Wang, Y., Shatir, S., Syed-Hassan, A., Su, S., Liu, C.Y., Xiang, J., 2016. Formation, fates and roles of catalytic precursors generated from the K_2CO_3–carbon interactions in the K_2CO_3–catalyzed CO_2 gasification of coal char. J. Anal. Appl. Pyrol. Online. http://dx.doi.org/10.1016/j.jaap.2016.11.006.
Kim, Y.S., Kim, Y.S., Kim, S.H., 2010. Investigation of thermodynamic parameters in the thermal decomposition of plastic waste-waste lube oil compounds. Environ. Sci. Technol. 44, 5313–5317.
Kopyscinski, J., Rahman, M., Gupta, R., Mims, C.A., Hill, J.M., 2014. K_2CO_3 catalyzed CO_2 gasification of ash-free coal interactions of the catalyst with carbon in N_2 and CO_2 atmosphere. Fuel 117, 1181–1189.
Lin, H.J., Rong, C.X., Jiu, B.B., Li, B.X., Yu, Q.J., Gan, L.H., Zhang, Z.Y., 2017. Effects of chromium on pyrolysis characteristic of water hyacinth (Eichornia crassipes). Energ. Online Renew. http://dx.doi.org/10.1016/j.renene.2017.08.045.
Liu, J.Y., Huang, S.J., Sun, S.Y., Ning, X.A., He, R.Z., Li, X.M., Chen, T., Luo, G.Q., Xie,

W.M., Wang, Y.J., Zhuo, Z.X., Fu, J.W., 2015. Effects of sulfur on lead partitioning during sludge combustion based on experiments and thermodynamic calculations. Waste Manage. 38, 336–348.
Luo, G.E., Strong, P.J., Wang, H.L., Ni, W.Z., Shi, W.Y., 2011. Kinetics of the pyrolytic and hydrothermal decomposition of water hyacinth. Bioresour. Technol. 102, 6990–6994.
Miranda, T., Román, S., Montero, I., Nogales-Delgado, S., Arranz, J.I., Rojas, C.V., González, J.F., 2012. Study of the emissions and kinetic parameters during combustion of grape pomace: dilution as an effective way to reduce pollution. Fuel Process. Technol. 103, 160–165.
Mishima, D., Kuniki, M., Sei, K., Soda, S., Ike, M., Fujita, M., 2008. Ethanol production from candidate energy crops: water hyacinth (*Eichhorniacrassipes*) and water lettuce (*Pistiastratiotes* L.). Bioresour. Technol. 99, 2590–2600.
Muhammad, S.B., Peter, A.J., Flemming, F., Stig, W., Kim, D.J., Johan, W., Søren, T.P., 2012. Ash transformation and deposit build-up during biomass suspension and grate firing: full-scale experimental studies. Fuel Process. Technol. 97, 93–106.
Otero, M., Sánchez, M.E., Gómez, X., 2011. Co-firing of coal and manure biomass: a TG-MS approach. Bioresour Technol. 102, 8304–8309.
Sebestyén, Z., Barta-Rajnai, E., Bozi, J., Blazsó, M., Jakab, E., Miskolczi, N., Sója, J., Czégény, Z.S., 2017. Thermo-catalytic pyrolysis of biomass and plastic mixtures using HZSM-5. Appl. Energ. Online.
Shao, J.G., Yan, R., Chen, H.P., Yang, H.P., Lee, D.H., 2010. Catalytic effect of metal oxides on pyrolysis of sewage sludge. Fuel Process. Technol. 91, 1113–1118.
Shen, B.X., Qin, L., 2006. Study on MSW catalytic combustion by TGA. Energ. Convers. Manage. 47, 1429–1437.
Sutton, D., Kelleher, B., Ross, J.R.H., 2001. Review of literature on catalysts for biomass gasification. Fuel Process Technol. 73, 155–173.
Vamvuka, D., Salpigidou, N., Kastanaki, E., Sfakiotakis, S., 2009. Possibility of using paper sludge in co-firing applications. Fuel 88, 637–643.
Villamagna, A.M., Murphy, B.R., 2010. Ecological and socio-economic impacts of invasive water hyacinth (Eichhorniacrassipes): a review. Freshwater Biol. 55, 282–298.
Xu, Y., Chen, B., 2013. Investigation of thermodynamic parameters in the pyrolysis conversion of biomass and manure to biochars using thermogravimetric analysis. Bioresour. Technol. 146, 485–493.
Xu, X.Y., Zhao, B., Sun, M.L., Chen, X., Zhang, M.C., Li, H.B., Xu, S.C., 2017. Co-pyrolysis characteristics of municipal sewage sludge and hazelnut shell by TG-DTG-MS and residue analysis. Waste Manage. 62, 91–100.
Yu, Z.S., Ma, X.Q., Liu, A., 2008. Kinetic studies on catalytic combustion of rice and wheat straw under air- and oxygen-enriched atmospheres, by using thermogravimetric analysis. Biomass Bioenerg. 32, 1046–1055.
Yu, Z., Ma, X., Liu, A., 2009. Thermogravimetric analysis of rice and wheat straw catalytic combustion in air- and oxygen-enriched atmospheres. Energ. Convers. Manage. 50, 561–566.
Zhao, Y., Hu, H., Jin, L., He, X., Wu, B., 2011. Pyrolysis behavior of vitrinite and inertinite from Chinese Pingshuo coal by TG-MS and in a fixed bed reactor. Fuel Process. Technol. 92, 780–786.
Zhuo, Z., Liu, J., Sun, S., Sun, J., Kuo, J., Chang, K., Fu, J., Wang, Y., 2017. Thermogravimetric characteristics of textile dyeing sludge, coal and their blend in N_2/O_2 and CO_2/O_2 atmospheres. Appl. Therm. Eng. 111, 87–94.
Zimmels, Y., Kirzhner, F., Kadmon, A., 2009. Effect of circulation and aeration on wastewater treatment by floating aquatic plants. Sep. Purif. Technol. 66, 570–577.